OMS-DPM: *O*ptimizing the *M*odel *S*chedule for Diffusion Probabilistic Models

Enshu Liu [*1] **Xuefei Ning** [*1] **Zinan Lin** [*2] **Huazhong Yang** [1] **Yu Wang** [1]

Abstract

Diffusion probabilistic models (DPMs) are a new class of generative models that have achieved state-of-the-art generation quality in various domains. Despite the promise, one major drawback of DPMs is the slow generation speed due to the large number of neural network evaluations required in the generation process. In this paper, we reveal an overlooked dimension—model schedule—for optimizing the trade-off between generation quality and speed. More specifically, we observe that small models, though having worse generation quality when used alone, could outperform large models in certain generation steps. Therefore, unlike the traditional way of using a single model, using different models in different generation steps in a carefully designed *model schedule* could potentially improve generation quality and speed *simultaneously*. We design OMS-DPM, a predictor-based search algorithm, to optimize the model schedule given an arbitrary generation time budget and a set of pre-trained models. We demonstrate that OMS-DPM can find model schedules that improve generation quality and speed than prior state-of-the-art methods across CIFAR-10, CelebA, ImageNet, and LSUN datasets. When applied to the public checkpoints of the Stable Diffusion model, we are able to accelerate the sampling by 2× while maintaining the generation quality.

1. Introduction

Diffusion probabilistic models (DPMs) (Sohl-Dickstein et al., 2015; Ho et al., 2020; Song et al., 2020b) are a recently emerging paradigm of generative models, which learns an iterative denoising process to transform gaussian noise to clean data. DPMs have already outperformed (Dhariwal & Nichol, 2021) other alternatives like variational autoencoders (VAEs) (Kingma & Welling, 2013) and generative adversarial networks (GANs) (Goodfellow et al., 2020) on both generation quality and likelihood estimation. DPMs have been successfully applied to various tasks, including image generation (Ho et al., 2020; Dhariwal & Nichol, 2021), super-resolution (Li et al., 2022; Saharia et al., 2022), video generation (Ho et al., 2022), speech generation (Kong et al., 2020; Chen et al., 2020), and point cloud completion and generation (Luo & Hu, 2021).

However, one major drawback of DPMs is the slow sampling speed. Specifically, the generation process of DPMs can be viewed as solving diffusion stochastic differential equations (SDEs) or ordinary differential equations (ODEs) using time-dependent score functions of data distributions (Song & Ermon, 2019; Song et al., 2020b). Neural networks (NNs) are trained to evaluate the score function. To solve the differential equations, DPMs usually need to discretize the continuous sample trajectories to hundreds or thousands of steps, each with one NN inference. This causes the un-

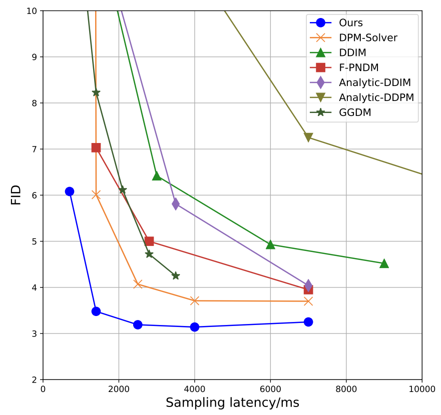

Figure 1. Generation quality v.s. latency on CIFAR-10. The horizontal axis is the time cost of generating a batch of images evaluated on a single NVIDIA A100 GPU (10 NFEs is approximately equivalent to 1400ms latency). The DPMs with model schedules derived by OMS-DPM achieves a significantly better trade-off than existing DPMs (Song et al., 2020a; Lu et al., 2022; Bao et al., 2022; Liu et al., 2022; Watson et al., 2022).

[*]Equal contribution [1]Department of Electronic Engineering, Tsinghua University, Beijing, China [2]Microsoft Research, Redmond, Washinton, U.S.A. Correspondence to: Xuefei Ning <foxdoraame@gmail.com>, Yu Wang <yu-wang@mail.tsinghua.edu.cn>.

Proceedings of the 40th International Conference on Machine Learning, Honolulu, Hawaii, USA. PMLR 202, 2023. Copyright 2023 by the author(s).

bearably slow sampling speed (up to 1000 times slower than GANs (Goodfellow et al., 2020; Song et al., 2020a)), making DPMs impractical for real-time applications. Prior work tackles this problem mostly by proposing better denoising formation, including *noise schedule*, *discretization scheme*, and *solver formula* (Song et al., 2020a;b; Liu et al., 2022; Zhang & Chen, 2022; Lu et al., 2022; Watson et al., 2021; Nichol & Dhariwal, 2021; Bao et al., 2022).

In this paper, we point out a *new* dimension for improving the trade-off between generation quality and speed—the *model schedule*. The key observation is that smaller models, though having worse generation quality when used alone, could outperform large models in certain denoising steps. Hence, unlike the common practice of using a single model, *using different models for different denoising steps* could potentially lead to benefits in *both* generation quality and speed. Therefore, the *model schedule*, the model assignments to each of the denoising steps, is an important factor to consider in DPMs.

Since the training and sampling of DPMs can be decoupled (Song et al., 2020a;b), using public pre-trained DPMs (e.g., Stable Diffusion (Rombach et al., 2022)) instead of training from scratch has become prevalent across academia and industry, and we expect to see more pre-trained DPMs to come in the future. Therefore, among all research directions around *model schedule*, we study the following problem:

Given a set of pre-trained DPM models and a generation time budget, how can we find the model schedule that optimizes the generation quality?

The problem is challenging due to the large search space that grows exponentially with respect to the number of steps. To address the challenge, we propose a method to Optimize the Model Schedule for Diffusion Probabilistic Model through predictor-based search (*OMS-DPM*). Our predictor takes the model schedule as input and predicts the generation quality. The predictor is trained with a small amount of data and can generalize to unseen model schedules. Equipped with the predictor, we employ an evolutionary algorithm to quickly explore the space and derive the well-performing model schedules under a wide range of generation time budgets.

Our contributions are as follows.

- Sec. 3: We point out an overlooked dimension—model schedule—for optimizing both the generation quality and sampling speed of DPMs. Specifically, we reveal the phenomenon where globally better models do not necessarily perform better on each individual denoising step, and using different models at different steps can lead to a significant improvement in generation quality and speed.
- Sec. 4: We propose an actionable method, OMS-DPM, to decide the model schedule that optimizes the generation quality given an arbitrary generation time budget. As OMS-DPM focuses on a novel optimizing dimension (i.e., the model schedule), it is orthogonal and compatible with existing methods that accelerate DPM sampling, including DDIM (Song et al., 2020a) and DPM-Solver (Lu et al., 2022). Specifically, OMS-DPM supports searching the special parameters in these methods such as step-skipping in DDIM and the solver order in DPM-Solver.
- Sec. 5: We experimentally validate OMS-DPM across a wide range of datasets, including CIFAR-10, CelebA, ImageNet-64 and LSUN-Church, and show that OMS-DPM can achieve significantly better trade-offs on generation quality and speed than the baselines (Fig. 1). For example, we are able to obtain model schedules that *simultaneously* achieve better FID (3.19 v.s. 3.56) and sampling speed (2.8× times faster) than using a single model (Ho et al., 2020) with DPM-Solver on CIFAR-10. To further demonstrate the practical value, we apply OMS-DPM on the 4 public checkpoints of the popular Stable Diffusion.[1] OMS-DPM is able to accelerate the sampling by over 2× while maintaining the generation quality on text-to-image generation task on MS-COCO 256×256 dataset (Lin et al., 2014). We have open-sourced our code at `https://github.com/jsttlgdkycy/OMS-DPM` to allow the community to use OMS-DPM.

2. Background and Related Work

2.1. Diffusion Probabilistic Models

Given a D-dimension random variable $x_0 \in \mathbb{R}^D$, Diffusion Probabilistic Models (DPMs) (Sohl-Dickstein et al., 2015; Ho et al., 2020) learns its distribution $q(x_0)$. DPMs define a *forward diffusion process* for x_t (Song et al., 2020b):

$$\mathrm{d}x_t = f(x_t, t)dt + g(t)dw_t, \tag{1}$$

where w_t is a standard Wiener process, and $x_0 \sim q(x_0)$. f and g determines the noise magnitudes in x_t. The *reverse diffusion process* from T to 0 is:

$$\mathrm{d}x_t = [f(t)x_t - g^2(t)\nabla_x \mathrm{log} q(x_t)]dt + g(t)\mathrm{d}\overline{w}_t, \tag{2}$$

where $x_T \sim q(x_T)$ and $\overline{w}_t$ is a reverse time standard Wiener process. This SDE has an equivalent probability flow ODE:

$$\mathrm{d}x_t = [f(t)x_t - \frac{1}{2}g^2(t)\nabla_x \mathrm{log} q(x_t)]\mathrm{d}t, \tag{3}$$

A NN (usually an U-net) is trained to learn $\nabla_x \mathrm{log} q(x_t)$. Then we can generate data by solving the reverse SDE or the ODE. Most DPM methods use one single NN to evaluate the score term. While some work proposes to uses multiple NNs for function evaluation at different timesteps (Jing

[1]https://huggingface.co/CompVis

et al., 2022; Balaji et al., 2022), they need to train the NNs only at their corresponding timesteps. In contrast, our work can utilize existing pre-trained NNs without inducing extra training cost.

2.2. Training-Free Samplers

To solve this ODE, one should first define f and g (i.e., *noise schedule*) and train neural networks (Nichol & Dhariwal, 2021). We often use α_t and σ_t to denote the *noise schedule*, which has a relationship with f and g as follows:

$$f(t) = \frac{\mathrm{dlog}\alpha_t}{\mathrm{d}t}, \quad g^2(t) = \frac{\mathrm{d}\sigma_t^2}{\mathrm{d}t} - 2\frac{\mathrm{dlog}\alpha_t}{\mathrm{d}t}\sigma_t^2. \quad (4)$$

Their ratio α_t/σ_t is called the signal-to-noise ratio (SNR). Then $[0, T]$ is discreted to timesteps $[t_0, t_1, \cdots, t_N]$, (i.e., *discretization scheme*). Finally *solver formula* is applied to compute each x_{t_i} at timestep t_i in order (Song et al., 2020a; Liu et al., 2022; Zhang & Chen, 2022; Lu et al., 2022). A training-free sampler only involves the last two parts of this solving process by utilzing pre-trained models. Many training-free samplers (Song et al., 2020a; Liu et al., 2022; Zhang & Chen, 2022; Lu et al., 2022) have been designed to achieve better trade-offs between the number of function evaluations (NFEs) and generation quality. They can be applied to any existing network (e.g., $\epsilon_\theta(x_t, t)$) without retraining. The following are two common samplers, both of which are compatible with our OMS-DPM.

DDIM (Song et al., 2020a) is one of the most popular samplers. Its solver formula is:

$$\begin{aligned} x_t = &\sqrt{\alpha_t}\frac{x_s - \sqrt{1-\alpha_s}\epsilon_\theta(x_s, s)}{\sqrt{\alpha_s}} \\ &+ \sqrt{1-\alpha_t-\sigma_s^2}\epsilon_\theta(x_s, s) + \sigma_s\epsilon_s, \end{aligned} \quad (5)$$

where $\epsilon_s \sim \mathcal{N}(\epsilon|0, \boldsymbol{I})$. There is no restriction on the value of s and t. However, big step sizes (small step numbers) often lead to large errors. When σ_s is set to zero, this solver is called **DDIM**.

DPM-Solver (Lu et al., 2022) gives a solver formula from x_s to x_t with a taylor expansion form :

$$\begin{aligned} x_t = &\frac{\alpha_t}{\alpha_s}x_s - \alpha_t\sum_{n=0}^{k-1}\epsilon^{(n)}(x_{\lambda_s}, \lambda_s)\int_{\lambda_s}^{\lambda_t} e^{-\lambda}\frac{(\lambda-\lambda_s)^n}{n!}\mathrm{d}\lambda \\ &+ \mathcal{O}((\lambda_t - \lambda_s)^{k+1}). \end{aligned}$$

It takes k NFEs to compute all derivatives. Besides, it applies a discretization scheme of uniform $\log(\mathrm{SNR})$, performing better than linear steps and quadratic steps.

2.3. AutoML

AutoML methods aim at automatically deciding for the optimal machine learning system respect to specific conditions such as task, dataset, and hardware. The research problems in the AutoML field include model selection, hyperparameter tuning and neural architecture design (Yang et al., 2019; Jaderberg et al., 2017; Zoph & Le, 2016). This work mainly focus on the automatic optimization of the proposed model schedule, including model selection and sampling schedule design for DPMs.

2.3.1. Predictor-based Neural Architecture Search

Neural Architecture Search (NAS) is an important sub-task of AutoML. NAS searches for suitable architectures under certain tasks and constraints (Zoph & Le, 2016; Elsken et al., 2019). One of the most challenging issues in NAS is the slow evaluation, due to the heavy computation burden of training and testing an architecture. Predictor-based NAS (Luo et al., 2018; Ning et al., 2020) is proposed to accelerate the evaluation phase, where a predictor is trained on a small number of architecture-performance pairs and can efficiently evaluate new architectures. In our problem, the evaluation of a DPM is expensive due to the slow sampling speed, and we borrow some ideas from NAS to propose a predictor-based method to accelerate the model schedule search.

3. Model Schedule: A New Dimension in DPM Design

Getting better trade-offs between the generation quality and speed of DPMs is an important problem that has drawn much attention. Since the only unknown term in Eq. (2) or Eq. (3) is the score term (i.e., $\nabla_x \mathrm{log}q(x_t)$), one can modify the sampling process after getting a pre-trained model used to estimate the score. Therefore, a lot of studies (Song et al., 2020a; Lu et al., 2022) have been focused on designing training-free samplers for the generation process, aiming to reduce the NFEs for generating high-quality samples. Different from existing studies, our work reveals a new dimension—model schedule—for training-free optimization of the DPMs' generation quality and speed. In this section, we discuss the motivation behind *model schedule*.

We start with a (perhaps surprising) observation that smaller models can actually outperform larger models at a wide range of denoising steps. We train a set of DPM models with different sizes on CIFAR-10 (Fig. 2). Unsurprisingly, using a single network with smaller latency across all steps leads to worse sample quality due to the lower model capacity (Fig. 2a). But the surprising observation is that the ranking of denoising ability is *not* consistent across the whole time axis (Fig. 2b). For example, architecture 1 with the worst overall generation quality actually outperforms most of the other models in the late denoising process. This observation also corroborates recent findings that different denoising

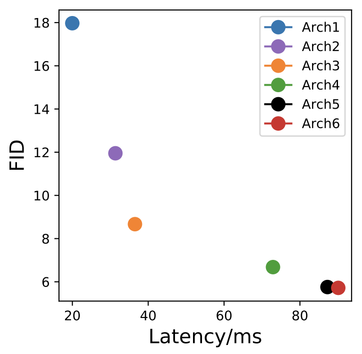

(a) Basic information of model zoo. The horizontal axis stands for the latency these neural architectures take to generate a batch of 128 images, testing on a single A100 GPU. The vertical axis stands for FID evaluated on 10k images generated through a 90-step DPM-Solver sampler (Lu et al., 2022) using these architectures alone as the score function estimator.

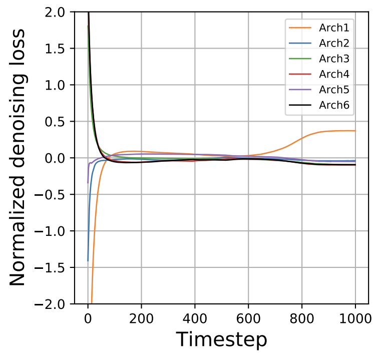

(b) Denoising loss on CIFAR-10 test set. The horizontal axis stands for different steps. The vertical axis stands for the denoising loss (lower is better, normalized for each step for better visualization). The models do not have a consistent ranking across all steps. A smaller model (thus having a smaller latency) could outperform larger models in some denoising steps.

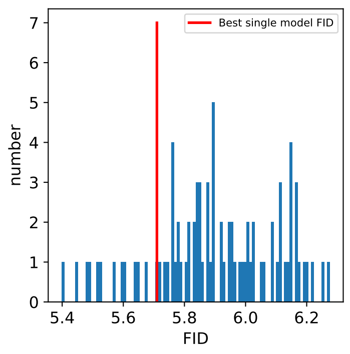

(c) Histogram of FIDs obtained by randomly combining models as the score function estimators for a 90-step DPM-Solver sampler (Lu et al., 2022). The red line indicates the best FID achieved by a single model in the model zoo (i.e., the lowest y-axis values of all points in Fig. 2a). This illustrates the value of mixing different models in the generation process of DPMs.

Figure 2. The importance of *model schedule* in DPM design.

steps perform different tasks (Yang et al., 2022; Choi et al., 2022).

This phenomenon sheds light on a new opportunity to improve the trade-off between *denoising loss* and *generation latency*. For example, if we replace the late denoising process of architecture 6 with architecture 1, we will get a smaller overall (denoising) loss and a smaller generation latency *simultaneously*, compared to using architecture 6 alone across all steps. Although a smaller denoising loss does not always indicate better generation quality (e.g., in FID) (Watson et al., 2021; Kim et al., 2021), we hypothesize that mixing different models across different steps could also benefit the trade-off between *generation quality* and *latency*. As a proof of concept, we randomly pick models in each of the denoising steps (Fig. 2c). We can obtain a model (with FID ≈ 5.4) that outperforms the model with the best generation quality in the model zoo (i.e., architecture 6) in terms of *both* generation quality and speed.

The phenomenon illustrated in Fig. 2 opens up new interesting research questions, including understanding when and why a DPM model would favor a specific denoising step, and how we can magnify it during *training* in an optimal way for the purpose of fast generation (e.g., by tuning loss weights (Song et al., 2021)). Given that using public pre-trained DPMs (e.g., stable diffusion (Rombach et al., 2022)) (instead of training new models from scratch) has become a popular paradigm, we study the following research question: assuming that we already have a set of pre-trained models, how we can decide the sequence of models to use, namely *model schedule*, to achieve the best trade-off between generation quality and latency.

4. OMS-DPM: Optimizing the Model Schedule

4.1. Problem Definition: Model Schedule Optimization

Suppose we have a pre-trained model zoo α with N models: $\alpha = \{a_1, a_2, \cdots, a_N\}$, where all a_is are neural networks trained to predict noise (Ho et al., 2020) or its variants (Sec. 2). Denote the inference latency of model a_i as l_i, the sampling time of the M-step DPM with a model schedule $a_{s_1}, a_{s_2}, \cdots, a_{s_M}$ placed on diffusion timesteps $t_1, t_2, \cdots, t_M$ can be estimated as $\sum_{m=1}^{M} l_{s_m}$, where $s_m \in \{1, \cdots, N\}$ is the model zoo index for the m-th denoising step. Giving a generation time budget C as the constraint, we aim to decide the number of sampling steps M and the model schedule that optimizes the sample quality:

$$\underset{\substack{M\le L,\\ a_{s_1},a_{s_2},\cdots,a_{s_M},\\ t_1,t_2,\cdots,t_M}}{\arg\min} \quad \mathcal{F}([(a_{s_1}, t_1), (a_{s_2}, t_2), \cdots, (a_{s_M}, t_M)]),$$

$$\text{s.t.} \sum_{i=1}^{M} l_{s_i} < C \tag{6}$$

where $\mathcal{F}([(a_{s_1}, t_1), (a_{s_2}, t_2), \cdots, (a_{s_M}, t_M)])$ refers to the sample quality score (e.g., FID) of using $a_{s_1}, a_{s_2}, \cdots, a_{s_M}$ at timesteps $t_1, t_2, \cdots, t_M$ respectively. L is the upper limit on the number of steps M. Note that the models are applied in the order of $a_{s_M}, a_{s_{M-1}}, \cdots, a_{s_1}$ to transform pure noises to data, i.e., $t_1 < t_2 < \cdots < t_M$.

The flexible optimization space in Eq. (6) contains several

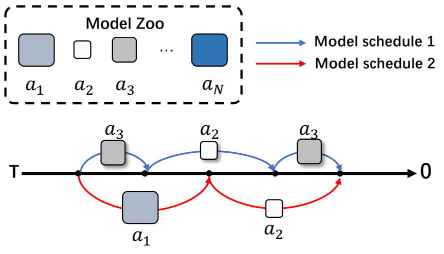

Figure 3. Illustration of two example model schedules.

dimensions: (1) The number of diffusion steps M. (2) The value of timesteps t_i (i.e., the discretization scheme). (3) The model a_{s_i} to apply at step t_i.

For deciding the timestep values, previous studies empirically discretize the timesteps *linearly* (Song et al., 2020a) or following the *uniform logSNR* principle (Lu et al., 2022). Song et al. (2020a) also propose a sub-sequence selection procedure that produces *quadratically* discretized timesteps. To solve Eq. (6), we follow previous empirical principles to discretize the timesteps beforehand: We designate the values for all L timesteps $t_1 \cdots t_L$ according to an empirical discretization scheme (*linear* (Song et al., 2020a) for DDIM experiments, and *uniform logSNR* (Lu et al., 2022) for DPM-Solver experiments). In order to support $M \leq L$ timesteps, we introduce a special type of model into the model zoo, *null model*, denoted as a_0. If a_0 is selected at a certain timestep, this timestep is unused in the reverse generation process. In this way, our optimization space contains a vast number of flexible timestep discretizations that are different from the manually designed ones in the literature. For instance, Fig. 3 illustrates two model schedules that can be derived from our optimization space, which have different timestep discretizations and different model choices.

After conducting the L-step discretization and introducing the null model, the optimization variables of problems are $\{s'_l\}_{l=1,\cdots,L}$, where $s'_l \in \{0, 1, \cdots, N\}$. The size of this optimization space is $(N+1)^L$, which is extremely large, e.g., about 10^{84} when $L = 100$ and $N = 6$.

Challenges. One simple idea is to use the model with the smallest loss on each timestep. However, as indicated in (Watson et al., 2021), loss values are not a good indication of the generation quality. To verify this, we run a 90-step DPM-Solver with the models with the minimal denoising loss at each step in Fig. 2b. This gives an FID of 8.56, worse than the random model schedules in Fig. 2c. A brute-force search method is also impractical due to the large search space and the evaluation overhead of $\mathcal{F}$. For example, it takes about 1 GPU hour to generate 5k samples (256×256 resolution), for evaluating only a *single* model schedule.

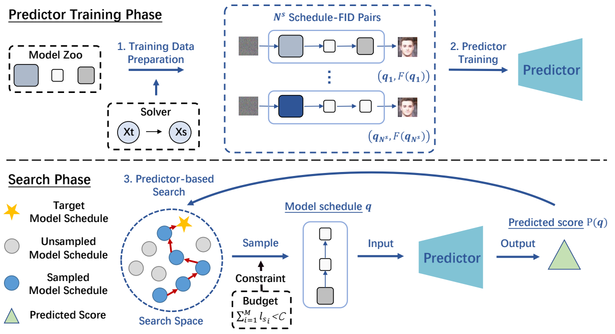

Figure 4. Our overall workflow contains 3 steps: (1) Prepare the data for predictor training. (2) Train the predictor. (3) Conduct the predictor-based evolutionary search. The inputs of our workflow include *model zoo*, *solver type*, and *budget*. *Budget* is only used in the search phase and does not affect the predictor training phase.

4.2. Predictor-based Model Schedule Optimization

To circumvent the above challenges, we propose to Optimize the Model Schedule for Diffusion Probabilistic Model through predictor-based search (OMS-DPM). We train a performance predictor that takes the model schedule as input and predicts its generation quality. This predictor can evaluate each model schedule in <1 GPU second, enabling us to solve the optimization problem efficiently. We'll first go through the workflow of our method in Sec. 4.2.1, and then elaborate on the predictor design in Sec. 4.2.2.

4.2.1. Overall Workflow

As shown in Fig. 4, we use the given model zoo[2] and ODE solver to (1) prepare the predictor training data and (2) use these data to train a performance predictor of model schedules. Then, for any given platform or budget, we can (3) run a predictor-based search to derive a suitable DPM. In the predictor-based search, the predictor will be used to evaluate model schedules sampled by an evolutionary algorithm. We will pick the model schedule with the best predicted score while satisfying the budget constraint.

Training Data Preparation. To prepare the data for predictor training, we randomly sample N^s (where the superscript s stands for *schedule*) model schedules $[\boldsymbol{q}_1, \cdots, \boldsymbol{q}_{N^s}]$ from the optimization space and evaluate their FID scores $\mathcal{F}(q_i)$. The sampling distribution for model schedules is designed to make the resulting sample quality scores diverse enough. To accelerate this phase, we only sample a few images to evaluate the FID. See App. C for the details. From this process, we get N^s pairs of model schedules and FID scores $\{(\boldsymbol{q_i}, \mathcal{F}(q_i))\}_{i=1,\cdots,N^s}$.

Predictor Training. Compared with the absolute quality,

[2]See App. B on how the model zoos can be obtained.

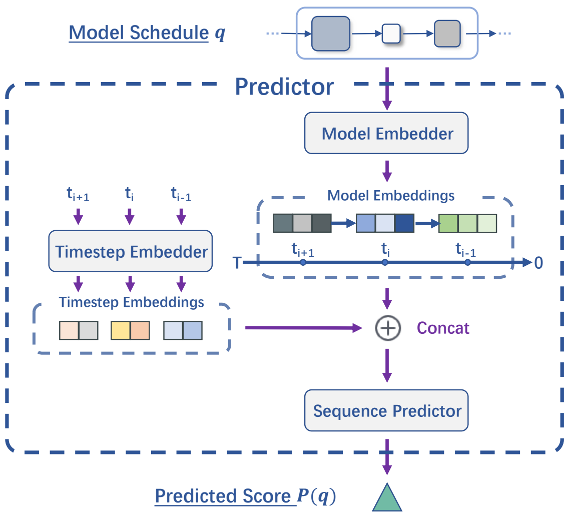

Figure 5. The predictor takes a model schedule $\boldsymbol{q}$ as input and predicts the generation quality $P(\boldsymbol{q})$. The predictor consists of a model embedder, a timestep embedder, and a sequence predictor.

the relative rankings of the model schedules are more important for guiding the search. Therefore, we adopt a pair-wise ranking loss (Ning et al., 2020) to train the predictor:

$$loss = \sum_{i=1}^{N^s} \sum_{j, F(\boldsymbol{q}_j) > F(\boldsymbol{q}_i)} \max(0, m - (\mathrm{P}(\boldsymbol{q}_j) - \mathrm{P}(\boldsymbol{q}_i))),$$

where m is the hinge compare margin. The ranking loss drives the predictor to preserve the relative ordering of predictions $\{P(\boldsymbol{q}_i)\}$ according to the true FID scores $\{F(\boldsymbol{q}_j)\}$. When predicting for an unseen model schedule, the lower the predicted score of a model schedule $\boldsymbol{q}$ is, the better generation quality we expect $\boldsymbol{q}$ to achieve.

Predictor-Based Evolutionary Search. Thanks to the predictor, we can use any search algorithm without incurring additional DPM training or evaluation overhead. We find that a simple evolutionary algorithm (Real et al., 2019) is sufficient for providing significant improvement. The algorithm iteratively modifies the current best model schedules (evaluated by the predictor) in the hope of finding better ones. The complete algorithm is provided in App. C.8.

Our OMS-DPM also supports searching the special parameters of the sampler (e.g., solver order in DPM-Solver); see App. C.2 for the details.

4.2.2. Predictor Design

Our predictor takes a model schedule $\boldsymbol{q}$ parametrized as $[s'_1, s'_2, \cdots, s'_L]$ as input and outputs a score for that schedule. As shown in Fig. 5, the predictor consists of a model embedder, a timestep embedder, and a sequential predictor.

Model Embedder. The model embedder maps a model choice $s'_l \in \{0, 1, \cdots, N\}$ to a $d^{\mathcal{M}}$-dimension continuous embedding $\mathrm{Emb}_l^{\mathcal{M}} \in \mathbb{R}^{d^{\mathcal{M}}}$ ($\mathcal{M}$ stands for *model*). Each model corresponds to a row in the globally trainable embedding matrix $\boldsymbol{O} \in \mathbb{R}^{(N+1)\times d^{\mathcal{M}}}$.

Timestep Embedder. The denoising functionality at each step is not only related to the model choice, but also the current timestep. Therefore, besides the model embedding, it is a logical choice to add timestep embedding as an additional input to our predictor. Our timestep encoder is an MLP that gets the sinusoidal embedding vector (Vaswani et al., 2017; Ho et al., 2020) from a single timestep scalar t_l and outputs the embedding $\mathrm{Emb}_l^{\mathcal{T}} \in \mathcal{R}^{d^{\mathcal{T}}}$ ($\mathcal{T}$ stands for timestep).

Sequence Predictor. After getting the model embeddings $[\mathrm{Emb}_1^{\mathcal{M}}, \cdots, \mathrm{Emb}_L^{\mathcal{M}}]$ and the timestep embeddings $[\mathrm{Emb}_1^{\mathcal{T}}, \cdots, \mathrm{Emb}_L^{\mathcal{T}}]$, we concatenate them at each timestep l to get $\mathrm{Feat}_l = (\mathrm{Emb}_l^{\mathcal{M}} | \ \mathrm{Emb}_l^{\mathcal{T}})$. Then the sequence $[\mathrm{Feat}_1, \cdots, \mathrm{Feat}_L]$ is input into an LSTM. The output features of the LSTM are averaged across timesteps and fed into an MLP to get the final score $\mathrm{P}(\boldsymbol{q})$.

5. Experiments

In this section, we first show the results of OMS-DPM with two popular samplers, DPM-Solver (Lu et al., 2022) and DDIM (Song et al., 2020a), on CIFAR-10, CelebA, ImageNet-64, and LSUN-Church datasets (Sec. 5.1). We then demonstrate the practical value of OMS-DPM with Stable Diffusion (Sec. 5.2). Ablation studies are provided in Sec. 5.3. We provide our empirical insights in Sec. 5.4. The model zoo information and experimental settings can be found in App. B and App. C.

Baselines. We use three types of baselines as listed below. **Baseline (1)** uses a single model across all timesteps and adopts common sampler settings (including timestep schedules or DPM-solver orders). Specifically, we first compute the steps S of using model a_i according to $S(C, i) = ceil(C/l_i)$ at each constraint C, where l_i means the latency of a_i and $ceil$ means upper rounding. We report the best FID among all models and in the model zoo using all sampler settings at every budget constraint C. Complete results and implementation details can be found at App. C.9. **Baseline (2)** is the model schedule with the best FID under budget constraint C in the training set. **Baseline (3)** is a randomly generated model schedule under budget constraint C. We run this process for 3 random seeds. The comparison with baseline **(1)** can illustrate the importance of mixing models, while the comparison with baseline **(2)** and **(3)** can illustrate the necessity of using a predictor and a search algorithm.

For our OMS-DPM, we run the search process with 3 random seeds and report the mean FID and the standard deviation. Information about the predictor can be found in Tab. 11. All predictors achieve a high Kendall's Tau (KD) with unseen validation data, indicating their reliability.

Budget/ms	**Baseline Type**			**Ours**
	(1)	**(2)**	**(3)**	
7.0×10^3	3.56	3.33	9.33±0.17	**3.25±0.01**
4.0×10^3	3.61	3.33	11.77±0.53	**3.14±0.02**
2.5×10^3	3.93	3.64	13.61±0.37	**3.19±0.05**
1.4×10^3	5.23	6.40	17.42±2.09	**3.48±0.06**
0.7×10^3	8.73	10.68	24.11±3.91	**6.08±0.00**

(a) Results on CIFAR-10

Budget/ms	**Baseline Type**			**Ours**
	(1)	**(2)**	**(3)**	
7.0×10^3	2.49	2.41	2.89±0.06	**2.13±0.03**
5.0×10^3	2.49	2.79	3.64±0.29	**2.12±0.03**
3.0×10^3	2.40	2.76	6.27±0.64	**2.17±0.03**
1.5×10^3	2.78	3.07	7.75±0.94	**2.42±0.06**
0.65×10^3	4.79	6.19	11.27±2.08	**3.53±0.22**

(b) Results on CelebA

Budget/ms	**Baseline Type**			**Ours**
	(1)	**(2)**	**(3)**	
12.0×10^3	12.99	13.03	19.88±1.62	**12.86±0.08**
8.0×10^3	13.44	13.38	25.77±2.21	**13.01±0.10**
5.0×10^3	14.00	14.33	30.79±1.44	**13.64±0.13**
2.0×10^3	18.20	19.25	37.70±2.58	**16.77±0.31**
0.8×10^3	29.59	43.21	47.62±2.13	**23.94±0.00**

(c) Results on ImageNet-64

Budget/ms	**Baseline Type**			**Ours**
	(1)	**(2)**	**(3)**	
35×10^3	11.97	10.79	22.53±0.84	**9.30±0.01**
25×10^3	12.02	10.79	40.55±7.02	**9.30±0.01**
15×10^3	12.03	10.84	47.87±14.31	**9.39±0.11**
10×10^3	13.23	10.84	68.53±14.28	**9.25±0.00**
4×10^3	32.23	32.57	135.05±11.59	**13.94±0.00**

(d) Results on LSUN-Church

Table 1. FIDs of our searched schedules on four datasets with DPM-Solver. Budget stands for the time cost limit of generating a batch of images. We report our results against three baselines mentioned before: **(1)** Using a single model in the model zoo and changing the NFE to meet the budget constraint. **(2)** The best schedule in the training set of the predictor. **(3)** Random sampling from the search space.

5.1. The Effectiveness of OMS-DPM

Tabs. 1 and 2 show the results with DPM-Solver and DDIM respectively. The key takeaways are:

The importance of model schedules. We can see that baseline (2) outperforms baseline (1) in many cases. This further confirms the observation in Fig. 2c where mixing multiple models in the generation process is better than the current practice of using a single model.

The importance of the predictor and the search algorithm in OMS-DPM. We see that our OMS-DPM always outperforms baseline (2) and baseline (3) by a large margin. These benefits indicate that our predictor is able to generalize from the limited training set, and the search algorithm is able to find a better model schedule that outperforms the best one in the training set.

The robustness of OMS-DPM across datasets, budgets, and samplers. Our OMS-DPM always outperforms baseline (1) across all datasets, budgets, and both samplers. For example, under DPM-Solver, OMS-DPM achieves a significant boost under low budgets (e.g., 6.08 v.s. 8.73 on CIFAR-10, 23.94 v.s. 29.59 on ImageNet-64, 13.94 v.s. 32.23 on LSUN-Church). As the budget increases and more NFEs can be used for the generation, the FID will decrease and converge to a value. We can see that OMS-DPM can further lower the converging FID of DPM-Solver by properly mixing models (e.g., 3.14 v.s. 3.56 on CIFAR-10, 9.25 v.s. 11.97 on LSUN-Church). Fig. 1 provides a comparison to more state-of-the-art methods, where we report the results of DDIM and DPM-Solver with our own implementation and take other results from the original paper (Bao et al., 2022; Liu et al., 2022; Watson et al., 2022). We see that OMS-DPM clearly achieves the best tradeoffs between generation quality and speed. These results demonstrate that OMS-DPM is robust across datasets and budgets, and works well with state-of-the-art samplers.

5.2. Results with Stable Diffusion

To further demonstrate the practical value of OMS-DPM, we test OMS-DPM on the text-to-image generation task using Stable Diffusion (Rombach et al., 2022). We use the four officially released models to construct the model zoo, and choose DPM-Solver as the sampler. We test our FID on MS-COCO 256×256 validation set (Lin et al., 2014). Because the four models share the same architecture and thus have the same latency, the time cost only depends on the number of timesteps, and we show NFE as the time cost budget. Detailed settings can be found at App. C.

Practical value of OMS-DPM. Tab. 3 shows that OMS-DPM can achieve a better FID with 12 steps than the best single model with 24 steps. Given the popularity of Stable Diffusion, OMS-DPM can potentially save a significant amount of computation resources for the community.

More insights on model schedule and more use cases of OMS-DPM. Note that the 4 checkpoints used here are from different training iterations of *the same model*. Therefore,

Budget/ms	Baseline Type			Ours
	(1)	(2)	(3)	
9.0×10^3	4.29	4.19	7.67±0.26	**3.80±0.06**
6.0×10^3	4.73	4.54	8.86±0.78	**4.07±0.06**
3.0×10^3	6.42	7.10	13.14±1.19	**5.20±0.01**
1.5×10^3	10.01	9.72	15.55±1.02	**8.24±0.20**
0.75×10^3	16.11	14.75	22.04±6.07	**12.34±0.31**

(a) Results on CIFAR-10

Budget/ms	Baseline Type			Ours
	(1)	(2)	(3)	
15×10^3	4.61	4.51	5.97±1.32	**3.62±0.06**
10×10^3	4.75	4.73	7.49±0.86	**3.71±0.04**
7.0×10^3	5.03	5.75	8.21±0.64	**3.99±0.06**
4.0×10^3	5.64	7.01	10.34±0.77	**4.75±0.03**
1.5×10^3	7.32	10.31	12.21±2.22	**7.07±0.13**

(b) Results on CelebA

Budget/ms	Baseline Type			Ours
	(1)	(2)	(3)	
20×10^3	14.74	14.78	20.08±0.63	**14.67±0.07**
15×10^3	15.12	14.81	23.84±0.65	**14.78±0.08**
10×10^3	16.12	16.42	26.77±2.01	**15.16±0.10**
5×10^3	19.47	20.57	33.11±2.51	**18.07±0.16**
2×10^3	26.91	30.48	40.44±0.87	**25.10±0.52**

(c) Results on ImageNet-64

Budget/ms	Baseline Type			Ours
	(1)	(2)	(3)	
55×10^3	11.72	11.24	23.33±1.04	**10.95±0.08**
40×10^3	11.73	11.65	31.22±0.70	**10.98±0.11**
25×10^3	12.05	13.15	40.59±9.16	**11.10±0.22**
10×10^3	14.77	17.80	50.28±13.17	**13.70±0.20**
4×10^3	25.27	67.49	57.97±4.55	**23.03±0.67**

(d) Results on LSUN-Church

Table 2. FIDs of our searched schedules on four datasets with DDIM.

Budget/NFE	Baseline Type		Ours
	(1)	(2)	
9	13.01	13.01	**12.90**
12	12.11	11.37	**11.34**
15	11.92	11.13	**10.72**
18	11.88	11.13	**10.68**
24	11.81	11.13	**10.57**

Table 3. FID on MS-COCO 256×256. All FIDs in the table are calculated between 30k images in validation set and 30k generated images guided with the same captions.

Budget/ms	Manner	Model Zoo Size		
		2	4	6
7.0×10^3	Baseline (2)	3.44	3.68	3.33
	Search	**3.37±0.01**	**3.49±0.02**	**3.25±0.01**
4.0×10^3	Baseline (2)	3.57	3.59	3.33
	Search	**3.36±0.02**	**3.42±0.00**	**3.14±0.02**
2.5×10^3	Baseline (2)	3.63	3.59	3.64
	Search	**3.29±0.01**	**3.39±0.04**	**3.19±0.05**
1.4×10^3	Baseline (2)	6.01	6.58	6.40
	Search	**3.99±0.01**	**3.67±0.03**	**3.48±0.06**
0.7×10^3	Baseline (2)	28.15	13.88	10.68
	Search	**6.05±0.00**	**6.25±0.36**	**6.08±0.00**

Table 4. Searched FIDs of composing fewer models.

this experiment generalizes our insights in Sec. 3: the phenomenon in Fig. 2b happens for different models with the same neural architecture, and mixing checkpoints from a single training process with OMS-DPM is also beneficial. This insight could lead to broader use cases of OMS-DPM: since it is common to save multiple checkpoints during the training process, any developer or user of DPMs can use OMS-DPM to boost the generation speed and quality.

5.3. Ablation Study

We study the influences of *model zoo size* and the *predictor training data size* using DPM-Solver on CIFAR-10.

Model Zoo Size N. Tab. 4 shows the FID results of OMS-DPM with different model zoo sizes. We can see that using the largest model zoo with $N = 6$ achieves the best results, and we see an improvement over the baseline across all model zoo sizes. Nevertheless, the $N = 2$ results are slightly better than $N = 4$. One potential reason is that $N = 2$ induces a smaller search space, and thus OMS-DPM can explore the search space more sufficiently.

Predictor Training Data Size. Tab. 5 shows the FID results using different data sizes for predictor training. Unsurprisingly, using less data to train the performance predictor results in degraded performances. But in all three cases, OMS-DPM still achieves better results than the baseline, indicating that we can make the predictor training phase more efficient while still obtaining promising results.

5.4. Empirical Observations

We summarize the observations on the model schedule pattern, hoping to provide some practical insights. Two of

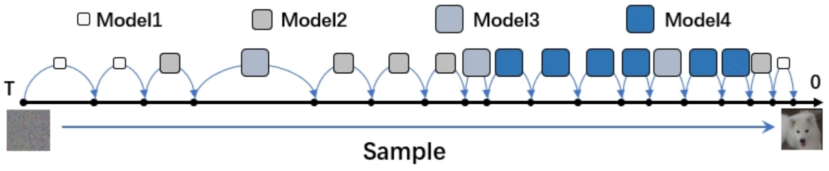

(a) A searched schedule on ImageNet-64 using DDIM under 2000ms budget.

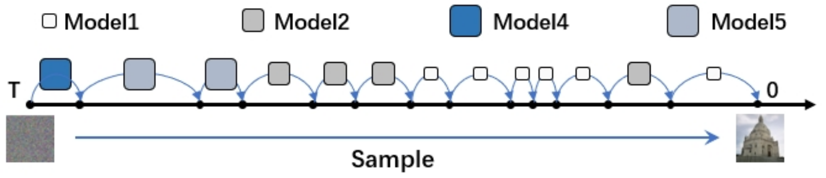

(b) A searched schedule on LSUN-Church using DDIM under 4000ms budget.

Figure 6. Two examples of searched schedules. The model numbers shown in the figure are consistent with the description at App. B. The sizes of model squares match the latencies of the corresponding models approximately.

our searched schedules are demonstrated in Fig. 6. More searched patterns can be found in Fig. 7.

Should we use more steps or larger models? Under a low time budget, using smaller models with more steps is more likely to gain a better generation quality than using larger models with fewer steps. The model schedules derived by OMS-DPM under the tightest budget (the last row of Tab. 1 and Tab. 2) are composed of only the 2 or 3 models with the lowest latency in the model zoo. This is because when the total number of steps is small, the error caused by the inexact solver formula and time discretization rises very quickly as the NFE decreases. Conversely, when having an adequate time budget, using larger models is suggested.

Should we apply larger models earlier or later? On ImageNet-64 with DPM-Solver and DDIM samplers and on CIFAR-10 with the DDIM sampler, using large models at steps near the generated data is more likely to achieve better performances than using large models at steps near the noise. Nevertheless, on LSUN-Church, the case is just the opposite. That is, using large models at steps near the noise is more likely to achieve better performances.

How should the timestep be discretized? For DDIM, we find the step size of our discovered schedules is larger at steps near the final generated image on CIFAR-10, CelebA, and ImageNet-64, especially on CelebA. On LSUN-Church, the step sizes at both ends are usually smaller than those in the middle part.

Which solver order should be used? For DPM-Solver, most of the discovered schedules apply the 1-st or 2-nd solvers under tight budgets. The 3-rd solver is only used under an adequate budget. For Stable Diffusion, our discovered schedules are mixed with 1-st, 2-nd, and 3-rd solvers under all budgets, and the 1-st solver is preferred when t is close to 0.

6. Limitations and Future Work

Although our method can efficiently derive specialized DPMs for any given budget, if given a new dataset or task, we need to prepare the predictor training data on that dataset or task and train a new predictor, which incurs a substantial overhead. Extending our method to be capable of efficiently deriving DPMs for new datasets and downstream tasks is an interesting future direction. Besides, as our experiments in Tab. 4 demonstrate that the quality and size of the model zoos matter for the performances, how to efficiently construct a good model zoo is a topic worth studying. For example, can we efficiently prune a pretrained model to get a diverse model zoo? Or can we design the ELBO loss weight (Choi et al., 2022; Kingma & Gao, 2023) to train a diverse model zoo?

Finally, let us take a broader perspective than deciding the best model schedule of pretrained models in DPM: As more and more open-source or proprietary models and APIs with varying expertise and complexity are coming forth, we believe the idea of cleverly combining off-the-shelf models and APIs to improve performance-efficiency trade-offs can support a wider range of applications.

Acknowledgements

This work was supported by National Natural Science Foundation of China (No. U19B2019, 61832007), Tsinghua University Initiative Scientific Research Program, Beijing National Research Center for Information Science and Technology (BNRist), Tsinghua EE Xilinx AI Research Fund, and Beijing Innovation Center for Future Chips. We thank Prof. Jianfei Chen, Tianchen Zhao, Junbo Zhao for their discussion.

References

Balaji, Y., Nah, S., Huang, X., Vahdat, A., Song, J., Kreis, K., Aittala, M., Aila, T., Laine, S., Catanzaro, B., et al. ediffi: Text-to-image diffusion models with an ensemble of expert denoisers. *arXiv preprint arXiv:2211.01324*, 2022.

Bao, F., Li, C., Zhu, J., and Zhang, B. Analytic-dpm: an analytic estimate of the optimal reverse variance in diffusion probabilistic models. *arXiv preprint arXiv:2201.06503*, 2022.

Chen, N., Zhang, Y., Zen, H., Weiss, R. J., Norouzi, M., and Chan, W. Wavegrad: Estimating gradients for waveform generation. *arXiv preprint arXiv:2009.00713*, 2020.

Choi, J., Lee, J., Shin, C., Kim, S., Kim, H., and Yoon, S. Perception prioritized training of diffusion models. In *Proceedings of the IEEE/CVF Conference on Computer Vision and Pattern Recognition*, pp. 11472–11481, 2022.

Dhariwal, P. and Nichol, A. Diffusion models beat gans on image synthesis. *Advances in Neural Information Processing Systems*, 34:8780–8794, 2021.

Elsken, T., Metzen, J. H., and Hutter, F. Neural architecture search: A survey. *The Journal of Machine Learning Research*, 20(1):1997–2017, 2019.

Goodfellow, I., Pouget-Abadie, J., Mirza, M., Xu, B., Warde-Farley, D., Ozair, S., Courville, A., and Bengio, Y. Generative adversarial networks. *Communications of the ACM*, 63(11):139–144, 2020.

Ho, J., Jain, A., and Abbeel, P. Denoising diffusion probabilistic models. *Advances in Neural Information Processing Systems*, 33:6840–6851, 2020.

Ho, J., Salimans, T., Gritsenko, A., Chan, W., Norouzi, M., and Fleet, D. J. Video diffusion models. *arXiv preprint arXiv:2204.03458*, 2022.

Jaderberg, M., Dalibard, V., Osindero, S., Czarnecki, W. M., Donahue, J., Razavi, A., Vinyals, O., Green, T., Dunning, I., Simonyan, K., et al. Population based training of neural networks. *arXiv preprint arXiv:1711.09846*, 2017.

Jing, B., Corso, G., Berlinghieri, R., and Jaakkola, T. Subspace diffusion generative models. *arXiv preprint arXiv:2205.01490*, 2022.

Kim, D., Shin, S., Song, K., Kang, W., and Moon, I.-C. Soft truncation: A universal training technique of score-based diffusion model for high precision score estimation. *arXiv preprint arXiv:2106.05527*, 2021.

Kingma, D. P. and Gao, R. Understanding the diffusion objective as a weighted integral of elbos. *arXiv preprint arXiv:2303.00848*, 2023.

Kingma, D. P. and Welling, M. Auto-encoding variational bayes. *arXiv preprint arXiv:1312.6114*, 2013.

Kong, Z., Ping, W., Huang, J., Zhao, K., and Catanzaro, B. Diffwave: A versatile diffusion model for audio synthesis. *arXiv preprint arXiv:2009.09761*, 2020.

Li, H., Yang, Y., Chang, M., Chen, S., Feng, H., Xu, Z., Li, Q., and Chen, Y. Srdiff: Single image super-resolution with diffusion probabilistic models. *Neurocomputing*, 479:47–59, 2022.

Lin, T.-Y., Maire, M., Belongie, S., Hays, J., Perona, P., Ramanan, D., Dollár, P., and Zitnick, C. L. Microsoft coco: Common objects in context. In *European conference on computer vision*, pp. 740–755. Springer, 2014.

Liu, L., Ren, Y., Lin, Z., and Zhao, Z. Pseudo numerical methods for diffusion models on manifolds. *arXiv preprint arXiv:2202.09778*, 2022.

Lu, C., Zhou, Y., Bao, F., Chen, J., Li, C., and Zhu, J. Dpm-solver: A fast ode solver for diffusion probabilistic model sampling in around 10 steps. *arXiv preprint arXiv:2206.00927*, 2022.

Luo, R., Tian, F., Qin, T., Chen, E., and Liu, T.-Y. Neural architecture optimization. *Advances in neural information processing systems*, 31, 2018.

Luo, S. and Hu, W. Diffusion probabilistic models for 3d point cloud generation. In *Proceedings of the IEEE/CVF Conference on Computer Vision and Pattern Recognition*, pp. 2837–2845, 2021.

Nichol, A. Q. and Dhariwal, P. Improved denoising diffusion probabilistic models. In *International Conference on Machine Learning*, pp. 8162–8171. PMLR, 2021.

Ning, X., Zheng, Y., Zhao, T., Wang, Y., and Yang, H. A generic graph-based neural architecture encoding scheme for predictor-based nas. In *European Conference on Computer Vision*, pp. 189–204. Springer, 2020.

Real, E., Aggarwal, A., Huang, Y., and Le, Q. V. Regularized evolution for image classifier architecture search. In *Proceedings of the aaai conference on artificial intelligence*, volume 33, pp. 4780–4789, 2019.

Rombach, R., Blattmann, A., Lorenz, D., Esser, P., and Ommer, B. High-resolution image synthesis with latent diffusion models. In *Proceedings of the IEEE/CVF Conference on Computer Vision and Pattern Recognition*, pp. 10684–10695, 2022.

Ronneberger, O., Fischer, P., and Brox, T. U-net: Convolutional networks for biomedical image segmentation. In *International Conference on Medical image computing and* *computer-assisted intervention*, pp. 234–241. Springer, 2015.

Saharia, C., Ho, J., Chan, W., Salimans, T., Fleet, D. J., and Norouzi, M. Image super-resolution via iterative refinement. *IEEE Transactions on Pattern Analysis and Machine Intelligence*, 2022.

Sen, P. K. Estimates of the regression coefficient based on kendall's tau. *Journal of the American statistical association*, 63(324):1379–1389, 1968.

Sohl-Dickstein, J., Weiss, E., Maheswaranathan, N., and Ganguli, S. Deep unsupervised learning using nonequilibrium thermodynamics. In *International Conference on Machine Learning*, pp. 2256–2265. PMLR, 2015.

Song, J., Meng, C., and Ermon, S. Denoising diffusion implicit models. *arXiv preprint arXiv:2010.02502*, 2020a.

Song, Y. and Ermon, S. Generative modeling by estimating gradients of the data distribution. *Advances in Neural Information Processing Systems*, 32, 2019.

Song, Y., Sohl-Dickstein, J., Kingma, D. P., Kumar, A., Ermon, S., and Poole, B. Score-based generative modeling through stochastic differential equations. *arXiv preprint arXiv:2011.13456*, 2020b.

Song, Y., Durkan, C., Murray, I., and Ermon, S. Maximum likelihood training of score-based diffusion models. *Advances in Neural Information Processing Systems*, 34: 1415–1428, 2021.

Vaswani, A., Shazeer, N., Parmar, N., Uszkoreit, J., Jones, L., Gomez, A. N., Kaiser, Ł., and Polosukhin, I. Attention is all you need. *Advances in neural information processing systems*, 30, 2017.

Watson, D., Ho, J., Norouzi, M., and Chan, W. Learning to efficiently sample from diffusion probabilistic models. *arXiv preprint arXiv:2106.03802*, 2021.

Watson, D., Chan, W., Ho, J., and Norouzi, M. Learning fast samplers for diffusion models by differentiating through sample quality. In *International Conference on Learning Representations*, 2022.

Yang, C., Akimoto, Y., Kim, D. W., and Udell, M. Oboe: Collaborative filtering for automl model selection. In *Proceedings of the 25th ACM SIGKDD international conference on knowledge discovery & data mining*, pp. 1173–1183, 2019.

Yang, X., Zhou, D., Feng, J., and Wang, X. Diffusion probabilistic model made slim. *arXiv preprint arXiv:2211.17106*, 2022.

Zhang, Q. and Chen, Y. Fast sampling of diffusion models with exponential integrator. *arXiv preprint arXiv:2204.13902*, 2022.

Zoph, B. and Le, Q. V. Neural architecture search with reinforcement learning. *arXiv preprint arXiv:1611.01578*, 2016.

Budget/ms	Manner	Training Data		
		915	**1831**	**3662**
7.0×10^3	Baseline (2)	3.49	**3.33**	3.33
	Search	**3.46±0.06**	3.34±0.07	**3.25±0.01**
4.0×10^3	Baseline (2)	3.43	3.33	3.33
	Search	**3.39±0.01**	**3.28±0.05**	**3.14±0.02**
2.5×10^3	Baseline (2)	3.64	3.64	3.64
	Search	**3.51±0.05**	**3.41±0.11**	**3.19±0.05**
1.4×10^3	Baseline (2)	7.41	7.01	6.40
	Search	**3.97±0.02**	**3.75±0.14**	**3.48±0.06**
0.7×10^3	Baseline (2)	10.68	10.68	10.68
	Search	**6.48±0.46**	**7.53±0.07**	**6.08±0.00**

Table 5. Searched FIDs of using less data for predictor training.

A. Additional Results

A.1. Results of ablation study

The results of our ablation study with less predictor training data are shown in Tab. 5.

A.2. Demonstration of searched model schedules

We show some searched schedules on all the four datasets using the two samplers at Fig. 7 (except for the searched patterns on ImageNet-64 and LSUN-Church using DDIM, which are shown at Fig. 6).

B. Model Zoo information

B.1. Model Zoo Construction

Leveraging a model zoo with varying complexities (models with different architectures) or functionalities (models with different architectures or training settings), our OMS-DPM method can derive model schedules that achieve superior speed-quality trade-offs. To obtain a model zoo, one can either construct and train the models themselves or directly use public models.

On CIFAR-10, CelebA, ImageNet-64, and LSUN-Church, in order to obtain models with varying complexities and functionalities, we adjust the model architectures and train the models ourselves. To be more specific, the most commonly used architecture family for DPMs is U-Net (Ronneberger et al., 2015; Ho et al., 2020; Song et al., 2020b; Dhariwal & Nichol, 2021). A U-Net is constructed by a series of downsampling stages and upsampling stages. All of these blocks consist of several residual blocks followed by a downsampling or upsampling block. In addition, a global attention head is used after all residual blocks in some stages. And we adjust the U-Net architecture by changing the **(1)** widths of each stage ("Channels" in Tabs. 6 to 9), **(2)** depth ("Depth" in Tabs. 6 to 9), including the number of stages and the number of residual blocks per stage, and **(3)** the number of the attention head ("Attention" in Tabs. 6 to 9). Then, we use the noise prediction form and linear noise schedule to train the models, and all other training settings are kept the same too. As the models have different architectures, they have different complexities and functionalities. In our experiments, the model zoo sizes are 6, 6, 7, and 6 on CIFAR-10, CelebA, ImageNet-64, and LSUN-Church, respectively.

While in the experiment of using Stable Diffusion (Rombach et al., 2022), we use the four officially provided pre-trained models at `https://huggingface.co/CompVis/stable-diffusion` to construct the model zoo.

More detailed architecture configurations and training settings are illustrated as following.

CIFAR-10. The architecture configurations are shown in Tab. 6. We choose the model 1,2,3,6 to construct the $N = 4$ model zoo and model 2,6 to construct the $N = 2$ model zoo in Sec. 5.3. We follow the training settings in (Ho et al., 2020). All models are trained with 128 batch size for 800k iterations, with a learning rate of 2×10^{-4}. We use 0.1 as dropout ratio and 0.9999 as EMA rate.

Number	Channels	Depth	Attention
1	32×[1,2,2,2]	2	1 head at 16×16
2	64×[1,2,2,2]	2	1 head at 16×16
3	128×[1,1,1]	1	-
4	128×[1,2,2,2]	2	-
5*	128×[1,2,2,2]	2	1 head at 16×16
6	128×[1,2,2,2]	2	4 heads at 16×16

Table 6. Architecture configuration on CIFAR-10. Model with * has the same architecture with the model used in (Ho et al., 2020).

CelebA. The architecture configurations are shown in Tab. 7. Following (Song et al., 2020a), we use a batch size of 128 and a learning rate of 2×10^{-4} for training. We train all models for 1000k iterations and save at every 50k, and then select the best among all checkpoints based on the FID with a 20-step DDIM sampler. We use 0.1 as dropout ratio and 0.9999 as EMA rate.

Number	Channels	Depth	Attention
1	32×[1,2,2,2,4]	2	1 head at 16×16
2	64×[1,2,2,2,4]	2	1 head at 16×16
3	64×[1,2,2,2,4]	3	1 head at 16×16
4*	128×[1,2,2,2,4]	2	1 head at 16×16
5	160×[1,2,2,2,4]	2	1 head at 16×16
6	128×[1,2,2,2,4]	3	1 head at 16×16

Table 7. Architecture configuration on CelebA. Model with * has the same architecture with the model used in (Song et al., 2020a).

ImageNet-64. The architecture configurations are shown in Tab. 8. We follow the architecture choice in (Nichol & Dhariwal, 2021), while we use our own settings for training. We set 128 as the batch size and 2×10^{-5} as the learning rate. We do not train models to predict varience like (Nichol & Dhariwal, 2021) does. We choose the checkpoints with 1500k iterations. Dropout ratio 0.1 and EMA rate 0.9999 are used.

LSUN-Church. The architecture configurations are shown in Tab. 9. We train these models with batch size 64 and learning rate 2×10^{-5}. We choose the checkpoints with 1000k iterations. Dropout ratio 0.1 and EMA rate 0.9999 are used.

Stable Diffusion. The four models we use share the same architecture but are trained on different datasets and have different parameters. All four models are latent diffusion models that contain three modules: (1) A pre-trained CLIP text encoder is used to encode the prompt information. (2) A VAE maps high-dimension images into a low-dimension latent space. (3) A DPM conducts generation in the latent space using a U-Net guided by the prompt encoding. Note that the four models share the same VAE and CLIP text encoder, so we can safely compose the four U-Nets for the latent diffusion process.

B.2. Inference Latency

We test the time cost of inferring a batch of data for all models by averaging the latency over 500 inferences, and all inferences are conducted on a single A100 GPU. We list all results in Tab. 10. The batch size b is 64 for LSUN-Church, 128 for CelebA and ImageNet-64, and 512 for CIFAR-10.

C. Experiment Details

C.1. Evaluation of DPMs

For the final evaluation of unconditional DPMs in Tabs. 1, 2, 4 and 5, we generate 50k images and calculate FID between the whole training set and the generated images. To reduce the randomness of evaluation for a fair comparison, we fix the

Number	**Channels**	**Depth**	**Attention**
1	32×[1,2,3,4]	3	1 head at 16×16 and 8×8
2	64×[1,2,3,4]	3	1 head at 16×16 and 8×8
3	96×[1,2,3,4]	3	1 head at 16×16 and 8×8
4	128×[1,2,3,4]	2	1 head at 16×16 and 8×8
5*	128×[1,2,3,4]	3	1 head at 16×16 and 8×8
6	128×[1,2,3,4]	4	1 head at 16×16 and 8×8
7	160×[1,2,3,4]	3	1 head at 16×16 and 8×8

Table 8. Architecture configuration on ImageNet-64. Model with * has the same architecture with the model used in (Nichol & Dhariwal, 2021).

Number	**Channels**	**Depth**	**Attention**
1	32×[1,1,2,2,4,4]	2	1 heads at 16×16
2	64×[1,1,2,2,4,4]	2	1 heads at 16×16
3	96×[1,1,2,2,4,4]	2	1 heads at 16×16
4	128×[1,1,2,2,4,4]	1	1 heads at 16×16
5	128×[1,1,2,2,4]	1	1 heads at 32×32
6*	128×[1,1,2,2,4,4]	2	1 heads at 16×16

Table 9. Architecture configuration on LSUN-Church. Model with * has the same architecture with the model used in (Ho et al., 2020).

50k generation noise in all our experiments. Since we use ODE samplers, there is no randomness in our evaluation. For experiments with stable-diffusion, we sample 30k captions in the validation set and use them to guide the generation with a guidance scale $s = 1.5$. Then we calculate the FID between generated images and the raw images of all sampled captions.

C.2. How to Conduct DPM Sampling for A Model Schedule

In this section, we explain how we conduct the DPM sampling corresponding to a specific model schedule $\boldsymbol{q} = [s'_1, \cdots, s'_L]$.

DPM-Solver. For DPM-Solver, a k-order DPM solver can be seen as grouping k timesteps together. Our problem parametrization can still be used: we group every 3 timesteps to form $L/3$ groups. For example, $a_{s_1}, a_{s_2}, a_{s_3}$ belong to the first group and will be used together in a single solver step. Note that for each group, our parametrization also enables us to decide between inactive solver (e.g., $s_1 = s_2 = s_3 = 0$), first-order (e.g., $s_1 \neq 0, s_2 = s_3 = 0$), second-order (e.g., $s_1 \neq 0, s_2 \neq 0, s_3 = 0$), and third-order DPM solvers. Finally, we divide the continuous time following *uniform logSNR* rule. The total number of time splits equals the number of used solver steps, or $L/3$ minus the number of inactive solvers. Consider an example schedule [1,2,3,3,0,0,0,0,0,1,2,0] with length 3×4. [1,2,3], [3,0,0], and [1,2,0] correspond to three solver steps, while [0,0,0] is not used during sampling. We split time [0,1] to four *solver timesteps* (three time splits) with *uniform logSNR*. We conduct a 2-nd order solver with model 2 and model 1 in order at the first split. Then we use a 1-st order solver with model 3 at the second split. Finally, we apply a 3-rd order solver using model 3, model 2, and model 1 in order at the last time split, and get the generated images.

We also adjust the sequence predictor to match the property of DPM-Solver. See App. C.4 for more details. For convenience, we set L to be divisible by 3 in our experiments with DPM-Solver.

For the maximum schedule length L, we set 90 on CIFAR-10 dataset, 60 on other datasets, and 45 for stable-diffusion.

DDIM. Different from the experiments with DPM-Solver, the search space in our experiments with DDIM contains the time discretization scheme. Specifically, we linearly discretized [0,T] beforehand to get L discrete timesteps. Then, the timesteps with non-zero s', $\{t_i | s'_i \neq 0\}_{i=1,\cdots,L}$, are used in sampling, while the other timesteps $\{t_i | s'_i = 0\}_{i=1,\cdots,L}$ don't invovle in sampling. We set L with DDIM as 200 on CelebA dataset and 100 on other datasets.

Number	**CIFAR-10**(ms)	**CelebA**(ms)	**ImageNet-64**(ms)	**LSUN-Church**(ms)
1	35.99±0.29	31.90±0.50	46.91±0.05	160.20±0.18
2	69.47±0.03	63.18±2.15	92.46±0.07	334.95±0.28
3	55.06±0.12	84.31±0.14	153.12±0.24	581.44±0.48
4	121.12±0.14	133.04±0.31	153.39±0.27	517.59±0.49
5	140.01±0.06	207.53±0.44	201.67±0.31	522.24±2.97
6	147.74±0.15	176.81±0.46	252.66±0.37	778.86±0.65
7	-	-	309.93±1.42	-

Table 10. Latency of all models in the model zoo.

C.3. Schedule-FID Data Generation

When generating schedule-FID data for predictor training, it's better to make the training data diversely distributed, such that the predictor can better generalize to unseen model schedules in the large search space. We set up multiple multinomial distributions by manually assigning the probabilities of picking each model from the model zoo. Then, for each multinomial distribution, we generate model schedules by sampling the model choice according to the distribution at each step. We will open source all the schedule-FID data for future use. For each model schedule on all unconditional generation tasks, we use the corresponding DPM to sample 5k images and evaluate the FID score. For experiments with stable-diffusion, we randomly sample 1.5k captions from the MS COCO 256×256 validation set for image generation, and then calculate the FID between generated images and the raw image of these sampled captions. Noting that the noise taken as input to generate schedule-FID data is also fixed.

C.4. Adjustment of the Sequence Predictor for DPM-Solver

DPM-Solver (Lu et al., 2022) uses a k-th solver to compute $x_{t_{i-1}}$ from x_{t_i}, which takes k NFE. So we make some adjustments to the sequence predictor module to match the characteristics of DPM-Solver. Specifically, we group each three model embeddings $[\mathrm{Emb}^{\mathcal{M}}_{i-2}, \mathrm{Emb}^{\mathcal{M}}_{i-1}, \mathrm{Emb}^{\mathcal{M}}_{i}]$ (i is divisible by 3), and then concatenate them to a $3M$-dimension encoding. We feed this encoding into a MLP to get an encoding that represents the combination of three models, which we call solver embedding. Finally, the solver embedding is concatenated with timestep embedding and fed into the LSTM.

C.5. Hyperparameter of Predictor

We set the model embedding dimension to 64 for ImageNet-64 as we use a larger model zoo size, and 32 for other datasets. For DPM-Solver, we set the solver embedding dimension to 64. For DDIM, we set the length of model embedding to 32. We used 64 as the dimension of timestep embedding. For the LSTM, we set the hidden size to 128 and the layer number to 1. Finally, we use an MLP with 4 layers and an output size of 200 at each layer except the last layer. No hyperparameter tuning is conducted.

C.6. Training

We use the ranking loss to train the predictor as described in Sec. 4.2.1. When obtaining a batch of b training data, we first randomly choose at most $compare\_ratio \times b$ pairs of data whose ground truth FID difference is larger than $threshold$. Then, we train the predictor with the ranking loss on these data. We set $compare\_ratio$ to 2, $threshold$ to 0.15 and the compare margin m to 1.0.

C.7. Validating the Reliability of Predictor

We use Kendall's Tau (KD) to evaluate the performance of predictor (Sen, 1968) . Specifically, we split our generated schedule-FID dataset into two parts: training set and validation set. We complete the training procedure on the training set and test the KD between predicted scores and ground truth FID on the validation set. We report our results in Tab. 11. And our predictor for stable-diffusion achieves a KD of 0.9543 on the validation set with 2070 training data and 108 validation data. Our predictors can achieve high KDs on unseen data, indicating their effectiveness.

Sampler	Dataset	Train	Valid	KD
DPM-Solver	CIFAR-10	3662	3662	0.9621
	CelebA	3460	3460	0.9461
	ImageNet-64	2735	2738	0.9611
	LSUN-Church	3082	884	0.9283
DDIM	CIFAR-10	3380	3380	0.9757
	CelebA	2660	2660	0.9653
	ImageNet-64	3240	360	0.9760
	LSUN-Church	1838	94	0.9675

Table 11. Information of all predictors. Train/Valid means the total num of data in the training/validation sets. KD means the Kendall's Tau on validation set between predicted score and true FID.

C.8. Evolutionary Search

Our complete search flow is shown at Algorithm 1. Time cost budget **C** should be given in advance. We first randomly initialize the whole schedule population P with a single model schedule as described in lines 1-3. To ensure the initial schedule $\boldsymbol{q}_0$ falls in a region with good quality, we ensure that it has a time cost in [0.9×**C**, **C**]. Then we conduct T loops, in each of which we sample a parent schedule from the current P and mutate the parent schedule to get a new candidate schedule. Specifically, we randomly sample at most $\mathbf{M}_{CP}$ schedules in the P as candidate parent set (denoted as CP) and choose the best one (denoted as $\boldsymbol{q}$ in line 8) as parent according to the predicted score. Then we mutate the parent to get more schedules denoted as $\boldsymbol{q_{new}}$ and add them into the next generation set (denoted as NG). The mutation is conducted for at most **iter** times or until the size of NG reaches $\mathbf{M}_{NG}$. Then all schedules in NG are added to the current population. If the size of P is more than $\mathbf{M}_P$, we eliminate excess according to the predicted score, as described in lines 18-19. Finally, after T loops, we choose the one with the best predicted score in the population as our searched schedule.

We set the maximum times **iter** of random mutation as 200 and the maximum population $\mathbf{M}_{NG}$ of the next generation as 40. The number **p** of candidate parents at every epoch is 10. The population cap $\mathbf{M}_P$ is set to 40. We set the total search epoch T as 600, but according to our experience, in most cases the search can reach the local optimum and be terminated around 200∼300 epochs.

C.9. Implementation Details and Full Results of Baseline (1)

We have reported the **best** FID achieved by DPMs using a single model and several common sampler settings (baseline **(1)**) under every budget in Sec. 5.1. The complete results of the generation quality are shown in Tab. 12 and Tab. 13. The full results support many of our analysis in Sec. 5.4. For example, smaller models converge more quickly at relatively lower budgets with worse convergence generation quality, and *quadratic* time discrete scheme is significantly better than *linear* time discrete scheme on CIFAR-10, CelebA and ImageNet-64 while the case is just the opposite on LSUN-Church. While the optimal hyper-parameters (e.g., the order of DPM-Solver, the time discretization scheme, the model size) are different for different datasets, our OMS-DPM can always outperform the baselines. This suggests the effectiveness of OMS-DPM in automatically finding good hyper-parameters and the benefits of reducing the burden of manual hyper-parameter tuning.

For DPM-Solver (Lu et al., 2022), we apply the fast version for 1-st, 2-nd and 3-rd order solver without adaptive step size based on the official implementation at `https://github.com/LuChengTHU/dpm-solver`. We apply *uniform logSNR* time discrete scheme following the default configuration.

For DDIM (Song et al., 2020a), we obtain the results by using *quadratic* time discrete scheme and *uniform* time discrete scheme on all four datasets, following the official implementation at `GitHub-ermongroup/ddim: DenoisingDiffusionImplicitModels`.

For stable-diffusion, we choose the single-step DPM-Solver and apply the *uniform logSNR* time discrete scheme. We also apply the fast version for 1-st, 2-nd and 3-rd order solver and choose the best one. Other settings are kept consistent with the default configuration of the official implementation at `GitHub-CompVis/stable-diffusion:`

Budget/ms	Model Number					
	1	2	3	4	5	6
7.0×10^3	15.89/15.54/15.54	10.62/9.83/9.84	7.56/6.59/6.57	6.36/4.65/4.62	5.24/3.74/3.70	5.29/3.57/**3.56**
4.0×10^3	16.23/15.53/15.56	8.49/6.60/6.60	11.36/9.83/9.83	8.09/4.72/4.56	7.13/3.84/3.71	7.38/3.63/**3.61**
2.5×10^3	16.77/15.49/15.51	10.19/6.65/6.56	12.58/9.84/9.84	11.44/4.81/4.64	10.74/4.17/4.07	11.09/3.95/**3.93**
1.4×10^3	18.26/15.46/15.51	14.11/6.92/6.81	15.72/10.01/9.75	22.57/8.09/**5.23**	22.95/6.70/6.01	24.25/7.41/6.89
0.7×10^3	22.49/15.69/15.74	28.68/**8.73**/12.22	27.59/11.44/10.10	50.29/39.04/23.07	60.33/69.40/289.53	56.55/43.14/297.67

(a) Full results on CIFAR-10

Budget/ms	Model Number					
	1	2	3	4	5	6
7.0×10^3	8.79/8.66/8.67	4.07/3.30/3.31	3.63/2.82/2.81	5.30/3.55/3.52	4.57/2.73/2.53	4.56/2.53/**2.49**
5.0×10^3	8.86/8.64/8.66	4.41/3.30/3.32	4.05/2.83/2.80	6.41/3.56/3.54	5.54/2.80/2.50	5.55/2.60/**2.49**
3.0×10^3	9.70/8.64/8.66	5.31/3.29/3.30	5.10/2.84/2.77	8.32/3.52/3.60	8.50/3.68/2.76	8.51/2.92/**2.40**
1.5×10^3	9.81/8.52/8.70	14.11/6.92/6.81	8.34/3.24/**2.78**	17.59/4.53/6.63	22.34/9.13/79.20	18.30/5.04/10.83
0.65×10^3	9.81/8.52/8.70	18.44/**4.79**/6.84	22.26/10.19/80.42	45.06/151.41/352.54	42.44/316.57/333.59	43.94/305.22/314.81

(b) Full results on CelebA

Budget/ms	Model Number						
	1	2	3	4	5	6	7
12×10^3	40.73/40.36/40.66	23.75/23.30/23.67	18.67/17.86/18.13	17.40/16.58/16.89	15.89/14.79/14.94	15.77/1404/14.10	15.43/**12.99**/13.04
8.0×10^3	40.95/40.34/40.64	24.16/23.41/23.68	19.54/18.10/18.23	18.25/16.79/16.90	17.43/15.10/14.97	17.95/14.49/14.34	18.66/13.67/**13.44**
5.0×10^3	41.40/40.39/40.59	25.18/23.59/23.67	21.97/18.53/18.24	20.53/17.20/17.00	21.23/15.89/15.29	23.23/15.66/14.76	25.25/15.19/**14.00**
2.0×10^3	43.87/40.65/40.62	31.74/25.26/23.96	36.74/21.79/19.51	35.99/20.50/**18.20**	46.09/23.92/20.63	57.25/30.84/33.40	66.38/30.80/41.10
0.8×10^3	52.35/41.79/42.59	59.70/33.86/**29.59**	81.26/52.18/42.97	82.16/57.88/39.99	120.38/276.14/254.11	118.21/250.15/243.33	162.16/209.78/209.77

(c) Full results on ImageNet-64

Budget/ms	Model Number					
	1	2	3	4	5	6
35×10^3	134.10/133.72/133.71	56.47/54.58/54.51	18.89/16.30/16.16	17.46/15.58/15.40	19.72/17.42/17.19	15.20/12.36/**11.97**
25×10^3	134.25/133.58/133.72	57.55/54.58/54.51	20.32/16.43/16.12	18.53/15.72/15.43	20.86/17.47/17.20	16.85/12.55/**12.02**
15×10^3	134.78/133.21/133.43	59.89/54.43/55.08	24.20/17.33/15.91	21.43/16.11/15.65	24.29/18.13/16.77	21.64/13.54/**12.03**
10×10^3	135.63/132.99/132.99	63.56/55.02/53.88	29.64/18.93/17.08	25.63/16.70/15.57	28.68/18.98/16.92	26.86/14.24/**13.23**
4.0×10^3	141.11/128.36/129.89	79.94/60.46/59.48	63.64/32.95/49.83	48.21/**32.23**/73.31	53.22/35.54/67.31	65.04/123.53/105.1

(d) Full results on LSUN-Church

Table 12. Complete FID results of baseline (1) using 1-st/2-nd/3-rd order of DPM-Solver on four datasets.

`Alatenttext-to-imagediffusionmodel`.

D. Generated Images

We put some samples using our method and baseline (1) under the lowest budget with DPM-Solver in this section at Fig. 8, Fig. 9, Fig. 10 and Fig. 11.

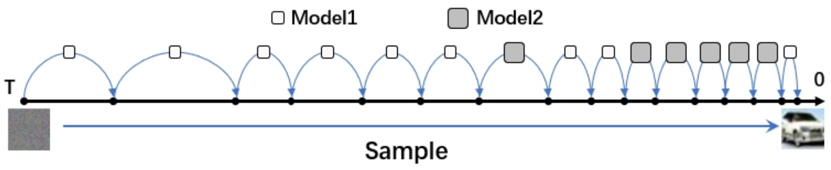

(a) A searched schedule on CIFAR-10 using DDIM under 750ms budget.

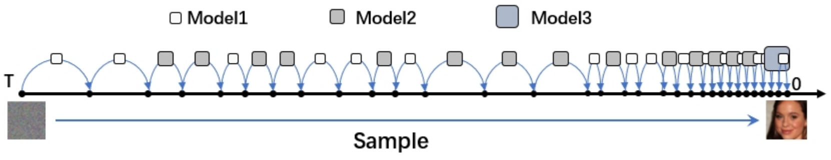

(b) A searched schedule on CelebA using DDIM under 1500ms budget.

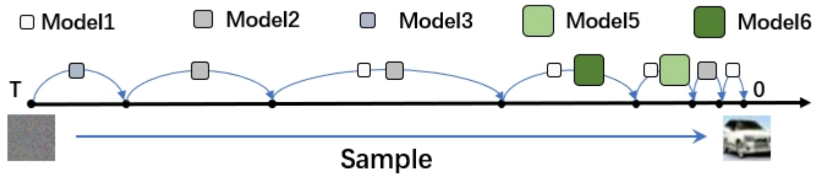

(c) A searched schedule on CIFAR-10 using DPM-Solver under 700ms budget.

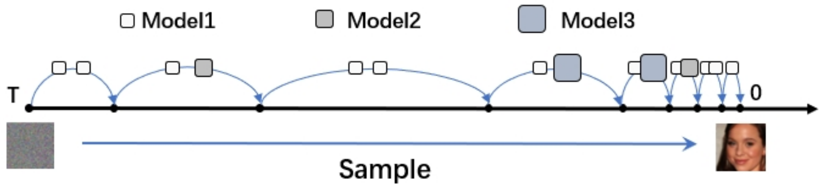

(d) A searched schedule on CelebA using DPM-Solver under 650ms budget.

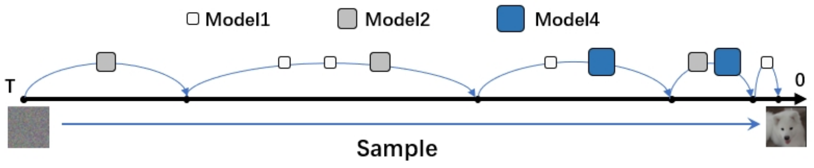

(e) A searched schedule on ImageNet-64 using DPM-Solver under 800ms budget.

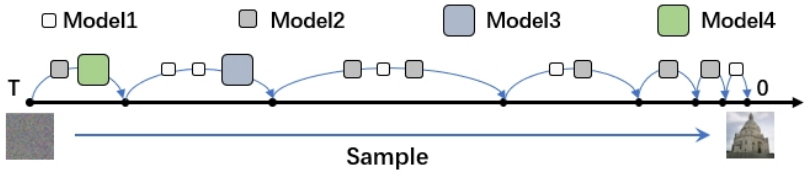

(f) A searched schedule on LSUN-Church using DPM-Solver under 4000ms budget.

Figure 7. Several examples of searched schedules. The model numbers shown in the figure are consistent with the description at App. B. The sizes of model squares match the latencies of the corresponding models approximately.

Algorithm 1 Predictor-based Evolutionary Search

```
Require:
    $\mathrm{Perf}()$: a trained predictor
    $GetCost()$: a function to get the time cost of a model schedule by summing inference latency of all the models.
Input:
    C: time budget of sampling a batch of images
Symbol:
    $P$: The whole Population of model schedule.
    $CP$: The Candidate Parents set of each loop, from which a parent model schedule is selected.
    $NG$: The Next Generation newly mutated from the parent schedule in each loop.
    $E$: The Eliminated model schedules in each loop.
Hyperparameter:
    Epoch: Number of loops for the entire search process.
    $\mathbf{M}_{CP}$: Maximum size of the candidate parents set $CP$.
    iter: Maximum number of mutations in each loop.
    $\mathbf{M}_{NG}$: Maximum size of the next generation set $NG$.
    $\mathbf{M}_P$: Maximum size of the whole population $P$.
Search Process:
 1: $P \leftarrow \varnothing$
 2: Initialize a Schedule $\boldsymbol{q}_0$
 3: Add $\boldsymbol{q}_0$ to $P$
 4: for $t = 1, \cdots,$ Epoch do
 5:     $i = 0$
 6:     $NG \leftarrow \varnothing$
 7:     Random Sample $min(\mathbf{M}_{CP}, |P|)$ model schedules from $P$, denoted as $CP$
 8:     Choose $\boldsymbol{q}$ with min $\mathrm{Perf}(\boldsymbol{q})$ in $CP$
 9:     while $i <$ itere and $|NG| < \mathbf{M}_{NG}$ do
10:         $\boldsymbol{q_{new}} \leftarrow$Randomly mutate $\boldsymbol{q}$
11:         if $GetCost(q_{new}) <$ C then
12:             add $\boldsymbol{q}_{new}$ to $NG$
13:         end if
14:         $i \leftarrow i + 1$
15:     end while
16:     $P \leftarrow P \cup NG$
17:     if $|P| > \mathbf{M}_P$ then
18:         Choose $|P| - \mathbf{M}_P$ model schedules denoted as $E$ with max $\mathrm{Perf}(\boldsymbol{q})(\boldsymbol{q} \in E)$ in $P$
19:         $P \leftarrow P - E$
20:     end if
21: end for
```

Budget/ms	**Model Number**					
	1	**2**	**3**	**4**	**5**	**6**
9.0×10^3	15.14/14.91	6.56/7.17	10.17/10.74	4.77/5.34	4.86/4.52	4.38/**4.29**
6.0×10^3	15.00/15.01	6.60/7.38	10.33/10.93	5.16/5.76	5.54/4.93	5.04/**4.73**
3.0×10^3	14.75/15.30	7.11/8.12	11.02/11.54	7.29/7.32	8.45/**6.42**	7.86/6.47
1.5×10^3	14.82/16.00	9.57/**10.01**	13.37/13.06	13.08/11.57	15.54/11.59	14.60/11.73
0.75×10^3	16.73/17.95	16.81/**16.11**	20.00/17.45	26.36/24.31	30.08/27.02	29.91/27.91

(a) Full results on CIFAR-10

Budget/ms	**Model Number**					
	1	**2**	**3**	**4**	**5**	**6**
15×10^3	8.44/9.79	4.74/5.57	4.63/5.19	6.48/4.98	6.51/**4.61**	6.48/4.88
10×10^3	8.46/9.81	5.42/5.62	5.53/5.25	7.78/5.10	8.04/**4.75**	7.98/5.04
7.0×10^3	8.57/9.84	6.36/5.69	6.54/5.33	9.08/5.30	9.71/**5.03**	9.49/5.37
4.0×10^3	8.92/9.85	8.22/5.89	8.88/**5.64**	11.48/5.97	12.28/5.92	11.80/6.30
1.5×10^3	10.74/9.97	13.12/**7.32**	13.90/7.75	15.61/9.65	17.07/11.93	15.84/12.83

(b) Full results on CelebA

Budget/ms	**Model Number**						
	1	**2**	**3**	**4**	**5**	**6**	**7**
20×10^3	41.91/42.29	24.41/25.71	19.18/19.82	18.11/18.66	16.57/16.61	16.05/15.71	15.08/**14.74**
15×10^3	42.07/42.31	24.64/25.78	19.53/19.96	18.46/18.78	16.95/16.81	16.55/16.04	15.67/**15.12**
10×10^3	42.44/42.40	25.01/25.96	20.12/20.32	19.53/19.17	17.71/17.29	17.53/16.74	16.81/**16.12**
5.0×10^3	43.36/42.72	26.05/26.61	21.73/21.78	20.76/20.50	20.12/**19.47**	20.66/19.95	20.78/20.13
2.0×10^3	45.49/44.06	29.13/29.74	27.56/28.34	**26.91**/27.00	30.77/31.38	36.25/37.36	40.09/41.49

(c) Full results on ImageNet-64

Budget/ms	**Model Number**					
	1	**2**	**3**	**4**	**5**	**6**
55×10^3	134.62/52.35	51.32/38.01	15.28/31.86	14.71/30.11	16.43/32.84	**11.72**/26.44
40×10^3	133.46/52.54	49.85/38.37	15.08/32.40	14.53/30.86	16.36/33.41	**11.73**/27.00
25×10^3	129.85/52.87	46.22/39.07	14.71/33.63	14.38/31.64	16.14/34.77	**12.05**/28.27
10×10^3	119.75/54.20	35.45/42.64	15.58/39.44	**14.77**/35.81	16.72/39.68	15.48/35.17
4.0×10^3	97.27/57.64	28.07/51.87	30.93/60.99	**25.27**/51.62	28.14/56.71	33.85/58.05

(d) Full results on LSUN-Church

Table 13. Complete FID results of baseline (1) using linear/quadratic time discretization scheme on four datasets with DDIM.

(a) Samples generated by the baseline (1) method. FID=8.73

(b) Samples generated by the OMS-DPM. FID=6.08

Figure 8. Samples of CIFAR-10 dataset under 700ms budget.

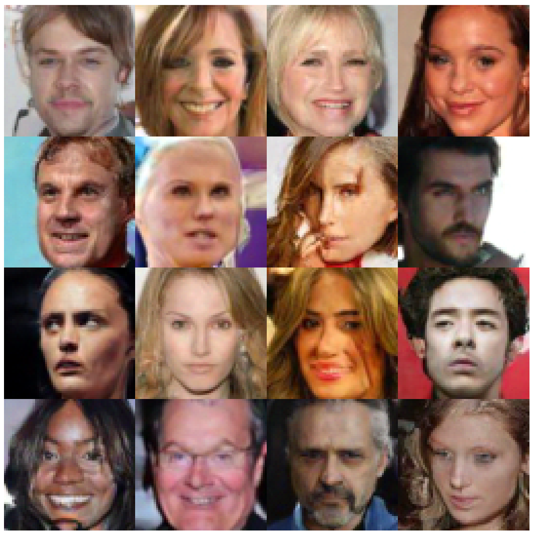
(a) Samples generated by the baseline (1) method. FID=4.79

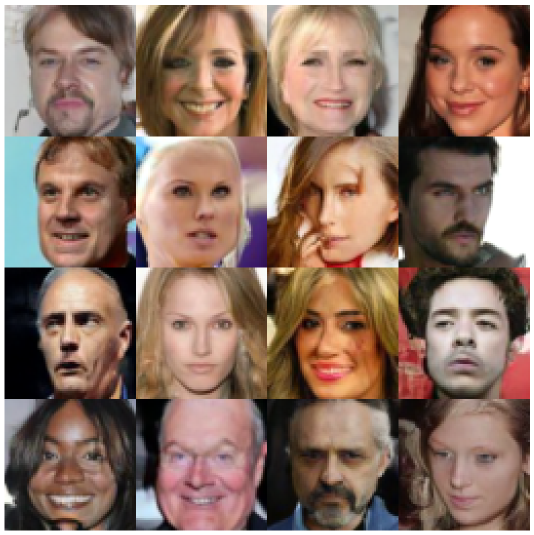
(b) Samples generated by the OMS-DPM. FID=3.53

Figure 9. Samples of CelebA dataset under 650ms budget.

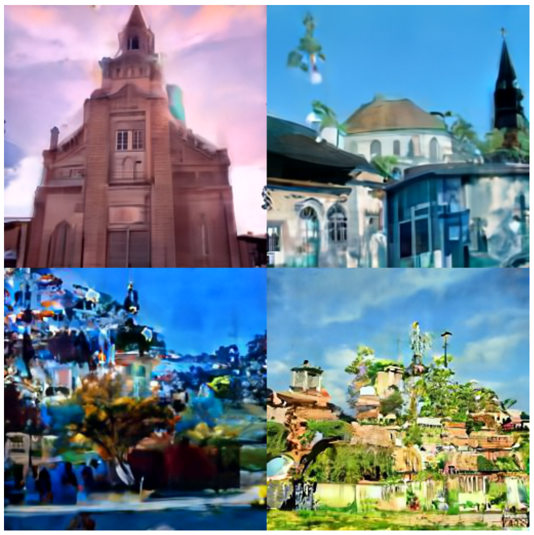
(a) Samples generated by the baseline (1) method. FID=32.23

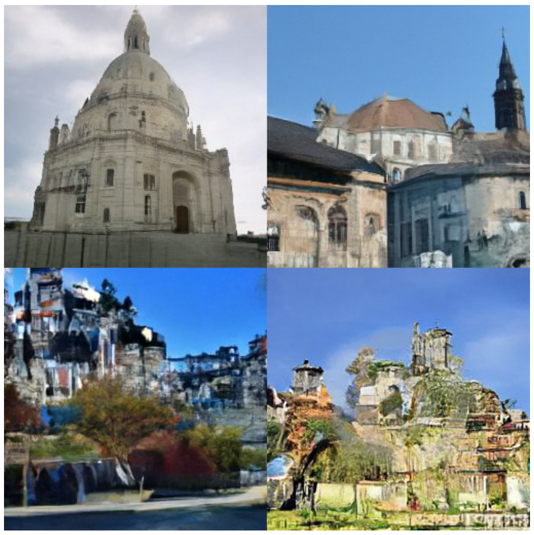
(b) Samples generated by the OMS-DPM. FID=13.94

Figure 10. Samples of LSUN-Church dataset under 4000ms budget.

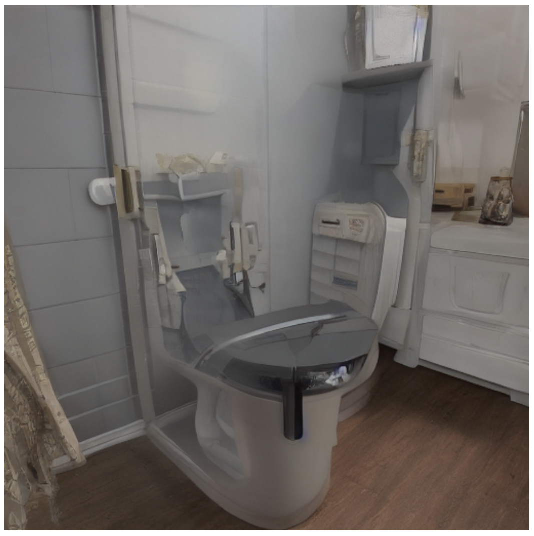
(a) Samples generated by the baseline (1) method. FID=11.92

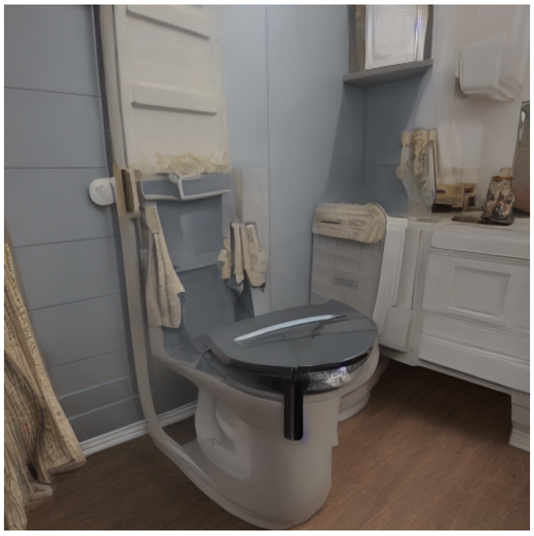
(b) Samples generated by the OMS-DPM. FID=10.72

Figure 11. Sample of MS-COCO 256×256 under 15 NFE budget, guided by the caption "A small closed toilet in a cramped space".